Journal of Power Sources 243 (2013) 33–39

Contents lists available at SciVerse ScienceDirect

Journal of Power Sources

journal homepage: www.elsevier.com/locate/jpowsour

Synthesis and electrochemical performance characterization of Ce-doped $Li_3V_2(PO_4)_3$/C as cathode materials for lithium-ion batteries

Jiexin Dang [a], Feng Xiang [a], Ningyu Gu [a], Rongbin Zhang [a], Rahul Mukherjee [b], Il-Kwon Oh [c], Nikhil Koratkar [b,d,*], Zhenyu Yang [a,b,*]

[a] Department of Chemistry, Nanchang University, No. 999, Xuefu Road, New District of Honggutan, Nanchang, Jiangxi 330031, PR China
[b] Department of Mechanical, Aerospace and Nuclear Engineering, Rensselaer Polytechnic Institute, 110 8th Street, Troy, NY 12180, USA
[c] Graphene Research Center, KAIST Institute of NanoCentury, School of Mechanical, Aerospace and Systems Engineering, Korea Advanced Institute of Science and Technology (KAIST), 291 Daehak-ro, Yuseong-gu, Daejeon 305-701, Republic of Korea
[d] Department of Materials Science and Engineering, Rensselaer Polytechnic Institute, 110 8th Street, Troy, NY 12180, USA

HIGHLIGHTS

- Synthesis of Ce-doped $Li_3V_2(PO_4)_3$/C cathode by microwave sol–gel route.
- At 1C, the Ce-doped cathode delivers a stable capacity of ~170 mAh g^{-1}.
- At 10C, the Ce-doped cathode delivers a stable capacity of ~120 mAh g^{-1}.

ARTICLE INFO

Article history:
Received 21 January 2013
Received in revised form
8 May 2013
Accepted 23 May 2013
Available online 8 June 2013

Keywords:
Lithium-ion batteries
Cathodes
Lithium transition metal phosphates
Cesium doping

ABSTRACT

In this paper, a series of Ce-doped $Li_3V_2(PO_4)_3$/C composite cathode materials for Li-ion batteries were synthesized by a facile and fast microwave assisted sol–gel route. The investigation of the influence of Ce doping on the structural and electrochemical characteristics of $Li_3V_2(PO_4)_3$/C shows that the resulting composite exhibits smaller particle size, lower electron-transfer resistance, and faster lithium ion migration, which are attributed to improved lithium ion transfer by the Ce doping. At low charge/discharge rates, the Ce-doped $Li_3V_{1.98}Ce_{0.02}(PO_4)_3$/C composite delivers a stable specific capacity of ~170 mAh g^{-1} for over 100 cycles. At high rates (e.g. 10C), the Ce-doped composite is still able to deliver stable capacities of up to ~120 mAh g^{-1} which is ~60% greater than its un-doped counterpart.

1. Introduction

Lithium ion batteries are considered to be the most promising rechargeable battery technology for EVs (electric vehicles) and electric energy storage from solar and wind energy sources [1,2]. The cathode material plays an important role in lithium-ion batteries, because its specific capacity is significantly less than graphitic anodes and its cost is a major contributor to the overall cost of the cell [3]. As of now, besides $LiCoO_2$, other cathode materials such as $LiFePO_4$, $LiMn_2O_4$, and $LiNi_{1/3}Co_{1/3}Mn_{1/3}O_2$ have been successfully brought to the market. In recent years, monoclinic $Li_3V_2(PO_4)_3$ has received extensive attention for Li-ion battery cathodes because of its high theoretical capacity and high operating voltage (up to 4.8 V) [4–8]. Furthermore, for monoclinic $Li_3V_2(PO_4)_3$, the structure of the slightly distorted VO_6 octahedra and PO_4 tetrahedra forms a unique three-dimensional framework [9], which provides a more efficient lithium ion diffusion channel in comparison to $LiFePO_4$ [10]. Moreover, the highly stable NASICON structure of $Li_3V_2(PO_4)_3$ endows the material with excellent cyclic stability [11]. However, like other lithium transition metal phosphates, the low electronic conductivity of $Li_3V_2(PO_4)_3$ adversely affects its overall electrochemical performance especially at high rates, and thus prevents its large-scale application in electric vehicles (EVs) and hybrid electric vehicles (HEVs).

* Corresponding authors. Department of Mechanical, Aerospace and Nuclear Engineering, Rensselaer Polytechnic Institute, 110 8th Street, Troy, NY 12180, USA. Tel.: +1 5182762630; fax: +1 5182762623.
E-mail addresses: koratn@rpi.edu (N. Koratkar), zyyang@ncu.edu.cn (Z. Yang).

0378-7753/$ – see front matter © 2013 Elsevier B.V. All rights reserved.
http://dx.doi.org/10.1016/j.jpowsour.2013.05.113

Significant efforts have been devoted to overcome the aforementioned drawbacks. Carbon coating [12,13] and cation doping [5,14–18] are two strategies that have been successfully used so far. Carbon coating does improve the surface electronic conductivity of $Li_3V_2(PO_4)_3$ but has no beneficial effect on the bulk phase lithium ion mobility and electron conductivity. By contrast, bulk phase characteristics can be remedied through cation doping approaches. Therefore carbon coating combined with cation doping may be a feasible way to improve the overall electrochemical performance of $Li_3V_2(PO_4)_3$. Despite the fact that many kinds of metallic ion doped $Li_3M_xV_{2-x}(PO_4)_3$/C (M = Cr^{3+}, Co^{2+}, Mg^{2+}, Al^{3+}, Nb^{5+}, etc.) [19–24] have been studied, the electrochemical performances of the composite electrode have not yet reached a satisfactory level.

Recently, Yang et al. [25] have developed a microwave solid-state synthesis route to prepare $Li_3V_2(PO_4)_3$ composites. The as-prepared sample after microwave heating for 5 min exhibits significantly improved electrochemical performance. Different from conventional solid state synthesis which involves sintering the target materials from the outside toward the inner core (which involves steep thermal gradients), microwave solid-state synthesis heats the material on the molecular level, leading to a uniform heating distribution. Considering the advantages associated with fast heating by microwave and the merits of carbon coating, there is great interest in developing an effective and fast Sol–gel process assisted by microwave heating to synthesize carbon-coated and cation doped $Li_3V_2(PO_4)_3$ cathode materials at low power and in short time.

Cerium (Ce) has a relatively large radius and high affinity for oxygen, and has been reported as an effective dopant for cathode materials in Li-ion battery. In this work, Ce^{3+} was introduced into the $Li_3V_2(PO_4)_3$/C complex as a partial substitute for V through a novel microwave-assisted sol–gel route. Based on this, the effects of Ce substitution on the electrochemical properties of $Li_3V_2(PO_4)_3$/C were investigated in detail.

2. Experiment

2.1. Preparation of $Li_3V_{2-x}Ce_x(PO_4)_3$/C samples

The $Li_3V_{2-x}Ce_x(PO_4)_3$/C cathode material (x = 0, 0.01, 0.02, 0.03, 0.05, 0.10) was synthesized by a sol–gel assisted microwave heating route in a molar ratio of Li:V:Ce:P = 3:2 − x:x:3 using Li_2CO_3, V_2O_5, $Ce(NO_3)_3$ and $NH_4H_2PO_4$ as raw materials. Citric acid was used as both chelating agent and carbon source which prevents the oxidation of vanadium ions and provides the networked structure of carbon for electronic conduction. All chemicals used in this paper were of analytical grade without any pretreatment.

First, V_2O_5, Li_2CO_3, $Ce(NO_3)_3$ and $NH_4H_2PO_4$ were mixed uniformly and dissolved in deionized water with continuous magnetic stirring at room temperature. After 4 h, a saturated aqueous solution of citric acid was added slowly with magnetic stirring until the solution turned light brown. In order to chelate the metal ions by citric acid, the pH value of above solution was adjusted to about 8.0–9.0 using $NH_3 \cdot H_2O$ until the solution color gradually turned brownish red. Subsequently, the mixture was heated to ~80 °C for ~12 h under active stirring for the purpose of evaporating the water until a blue colored gel was formed. Next, the precursor was obtained after drying at ~80 °C for ~24 h in an oven. Afterward, the as-prepared gel precursor was ground and sintered at ~450 °C for ~4 h in a flowing N_2 atmosphere. This allowed the formation and release of NH_3 and H_2O as well as CO_2 associated with the decomposition of organic components in the gel. Finally, the obtained precursor was carefully grounded after cooling to room temperature, and sealed in a crucible with a flowing N_2 atmosphere, and irradiated in a domestic microwave oven (2.45 GHz, 1000 W, Galanz microwave oven, China) at ~400 W for ~10 min to yield the $Li_3V_{2-x}Ce_x(PO_4)_3$/C composite.

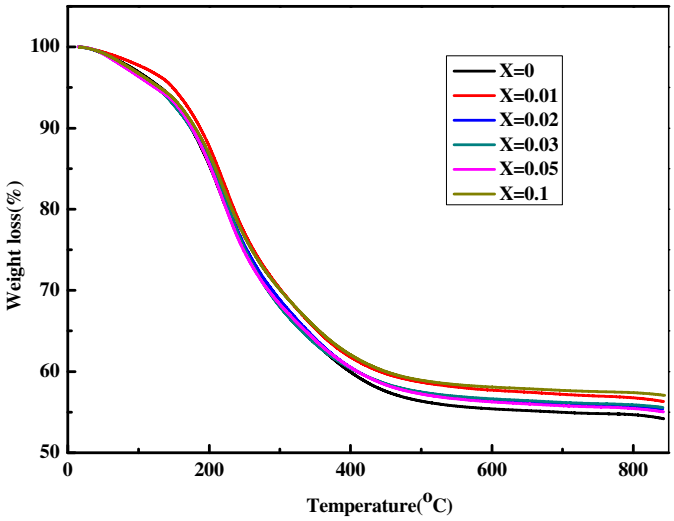

Fig. 1. TG curve for the dry gel precursor of $Li_3V_{2-x}Ce_x(PO_4)_3$/C (x = 0, 0.01, 0.02, 0.03, 0.05, 0.10) under N_2 flow at a heating rate of 10 °C min^{-1}.

2.2. Physical characterization

The crystalline structural characterization of the samples was carried out by X-ray diffraction (XRD) using a diffractometer (Philips X'Pert Pro Super, Cu K_α radiation), and the diffraction patterns were recorded at room temperature in the 2θ range between 10° and 60°. Thermogravimetric (TG) analysis was performed by using a SDTA851E thermoanalyzer using a heating rate of 10 °C min^{-1}. The morphology and particle sizes of the powders were characterized under a scanning electron microscope (SEM, JSM-6390LA) and transmission electron microscope (TEM, JEOL JEM-200CX, 200 kV).

2.3. Electrochemical testing

Electrochemical properties were evaluated with model CR2025 coin-type cell. Cycling and galvanostatic charge–discharge performance of the two-electrode electrochemical cells were tested on a

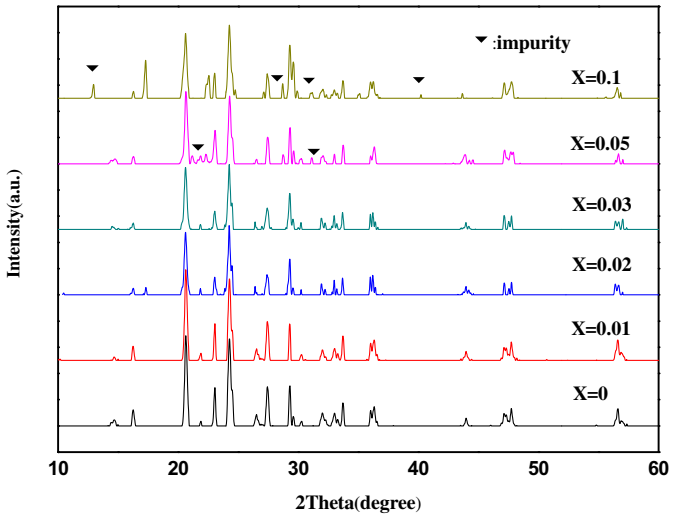

Fig. 2. XRD patterns of the $Li_3V_{2-x}Ce_x(PO_4)_3$/C (x = 0, 0.01, 0.02, 0.03, 0.05, 0.10) samples as a function of Ce^{3+} doping.

multi-channel battery test system (LAND, Wuhan) at different current densities in the voltage range between 3.0 and 4.8 V, while Cyclic voltammetry (CV) and electrochemical impedance spectroscopy (EIS) measurements were performed on an electrochemical workstation (Shanghai Chenhua CHI660C, China). For the two-electrode coin battery cell, a lithium metal foil of about 0.3 mm in thickness was used as the anode, and the cathode electrode was prepared as follows: The as-prepared powders, acetylene black and polyvinylidiene fluoride (PVDF) binder in a weight ratio of 82:10:8 were mixed in *N*-methyl-2-pyrrolidone (NMP) to create a slurry. The resulting slurry was coated on an Al current collector with a thickness of ~75 μm. The cathodes were dried in a vacuum furnace at 65 °C for ~20 h, following which they were roll-pressed at a pressure of ~15 MPa. Circular electrodes (12 mm in diameter) were then punched out. We measured the average weight of several pure aluminum sheets (12 mm in diameter), and the weight of the dry Al current collector (sheets) of the same size coated with the cathode materials. Then we computed the mass of the cathode materials by subtraction. The typical weight of the cathode ranged between ~7 and 8 mg. Finally, the cathode was dried again in a vacuum oven at ~100 °C for ~48 h prior to assembly. The cells were assembled in a high purity argon atmosphere inside a glove box (Mbraunlab Master130, Germany). Celgard® 2325 was used as the separator and the electrolyte was a solution of 1 M $LiPF_6$ dissolved in a mixture of ethylene carbonate (EC):dimethyl carbonate (DMC) (1:1 vol.%).

3. Results and discussion

3.1. TG analysis

Fig. 1 shows the thermogravimetric (TG) spectra for the dry gel precursor of $Li_3V_{2-x}Ce_x(PO_4)_3/C$ ($x = 0$, 0.01, 0.02, 0.03, 0.05, 0.1) in

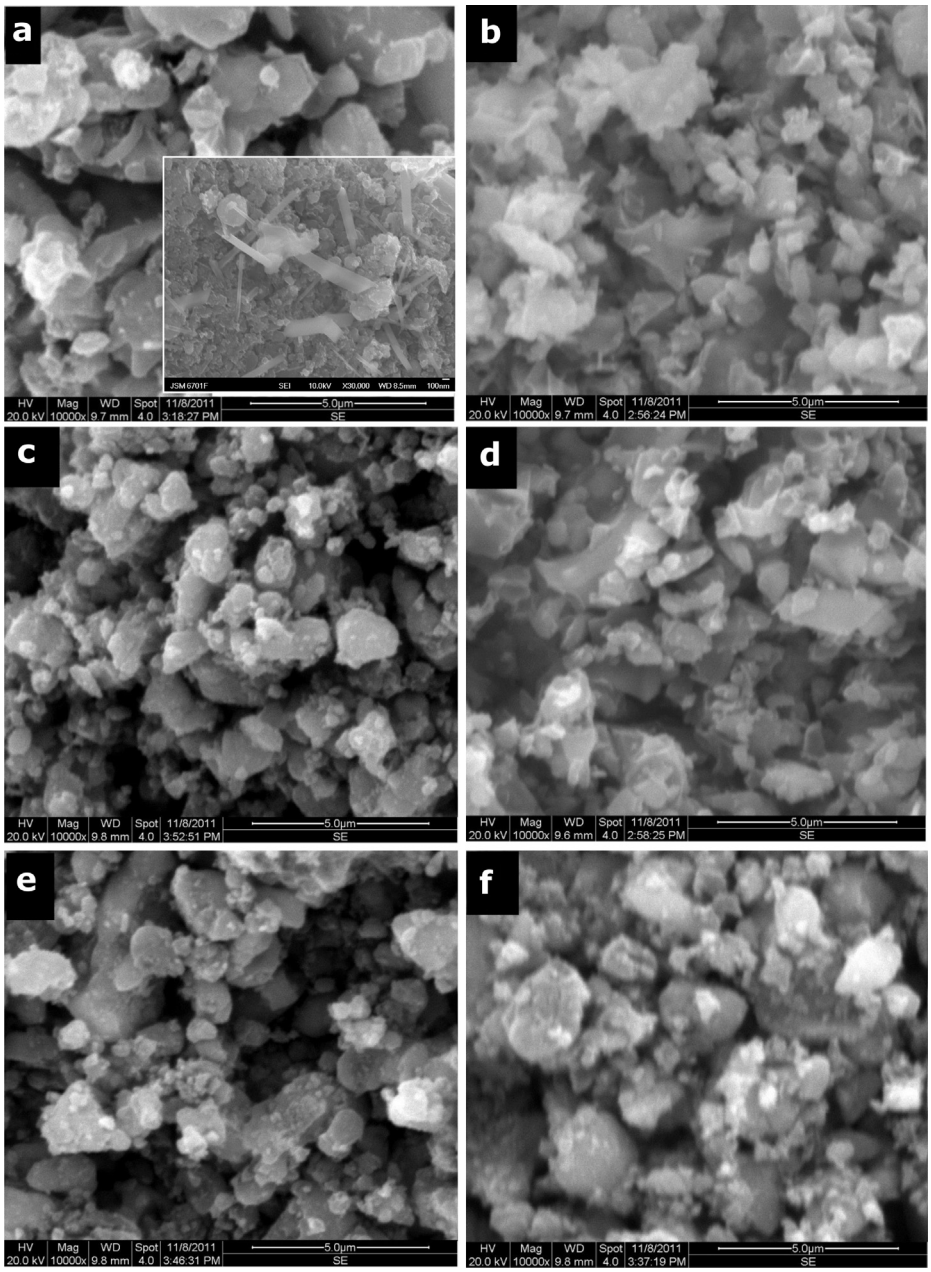

Fig. 3. SEM images of $Li_3V_{2-x}Ce_x(PO_4)_3/C$ samples with different Ce contents: (a) $x = 0$, the inset is a high-magnification image; (b) $x = 0.01$; (c) $x = 0.02$; (d) $x = 0.03$; (e) $x = 0.05$; (f) $x = 0.1$.

the temperature range between 25 °C and 850 °C under N_2 flow at a heating rate of ~10 °C min^{-1}. All the dry gel precursors of $Li_3V_{2-x}Ce_x(PO_4)_3$/C gave similar TG spectra. For the dry gel precursor of $Li_3V_{1.98}Ce_{0.02}(PO_4)_3$/C, about ~43% weight loss is observed during the temperature sweep to ~600 °C. Above ~600 °C, the weight loss becomes insignificant when the temperature was further increased to ~850 °C. There are three main weight loss stages in the TG curve, below 200 °C, 200–400 °C and 400–600 °C. It can be seen that the first stage shows an obvious weight loss peak near ~200 °C and the weight loss of the precursor is ~15.8 wt%, which is due to the loss of absorbed water and crystal water, hydrogen fluoride and ammonia escaping from the precursor. In the second stage of 200–400 °C, about 19.2 wt% of weight loss was observed, which can be attributed to the pyrolysis of citric acid. In the final stage, ~7.1% weight loss was observed due to the pyrolysis of the remaining organic compounds which occurs in the temperature range from 400 to 600 °C. Above 600 °C, there was no obvious weight loss in the TG curve, indicating that the chemical reactions have been completed and stable composites of $Li_3V_{2-x}Ce_x(PO_4)_3$/C were formed.

3.2. X-ray diffraction studies

XRD experiments are conducted to examine the structural changes to $Li_3V_{2-x}Ce_x(PO_4)_3$/C by incorporation of various amounts of Ce^{3+} (x = 0, 0.01, 0.02, 0.03, 0.05, 0.10). As shown in Fig. 2, the $Li_3V_{2-x}Ce_x(PO_4)_3$/C retained the single phase of un-substituted $Li_3V_2(PO_4)_3$/C up to x = 0.03. All fundamental peaks could be indexed to the typical monoclinic structure with space group P21/n(PDF 0074) [26], which indicates that Ce was successfully doped into the crystal lattice of $Li_3V_2(PO_4)_3$/C, and did not change the basic crystal structure of $Li_3V_2(PO_4)_3$/C. Therefore we expect that Ce^{3+} ions were located at the V^{3+} sites in the crystal lattice. Furthermore, the crystallinity of $Li_3V_2(PO_4)_3$ is maintained even after Ce doping. This factor is critical as high crystallinity has the potential to

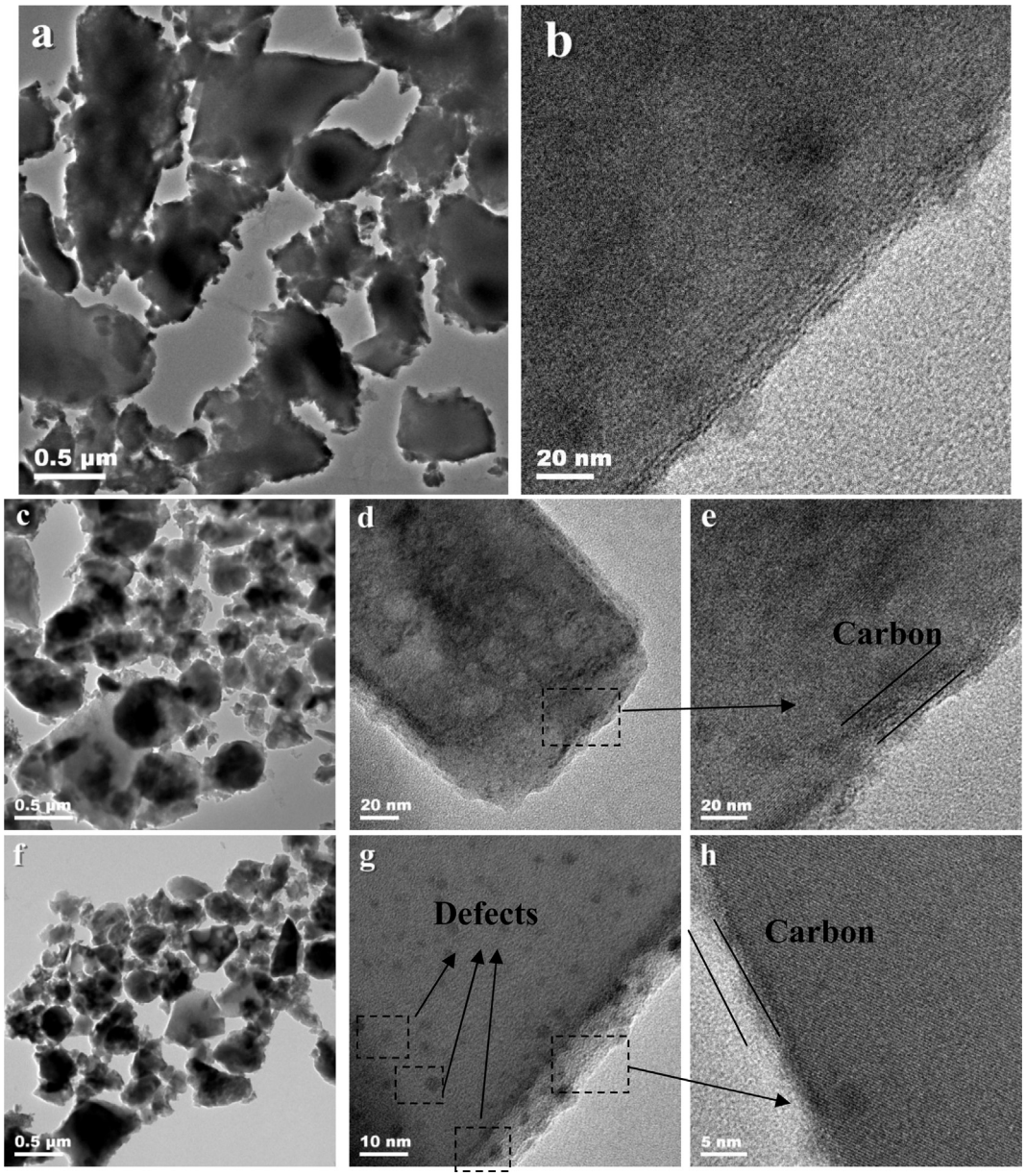

Fig. 4. TEM images of (a) $Li_3V_2(PO_4)_3$; (c) $Li_3V_2(PO_4)_3$/C; (f) $Li_3V_{1.98}Ce_{0.02}(PO_4)_3$/C and HRTEM images of (b) $Li_3V_2(PO_4)_3$; (d) and (e) $Li_3V_2(PO_4)_3$/C; (g) and (h) $Li_3V_{1.98}Ce_{0.02}(PO_4)_3$/C.

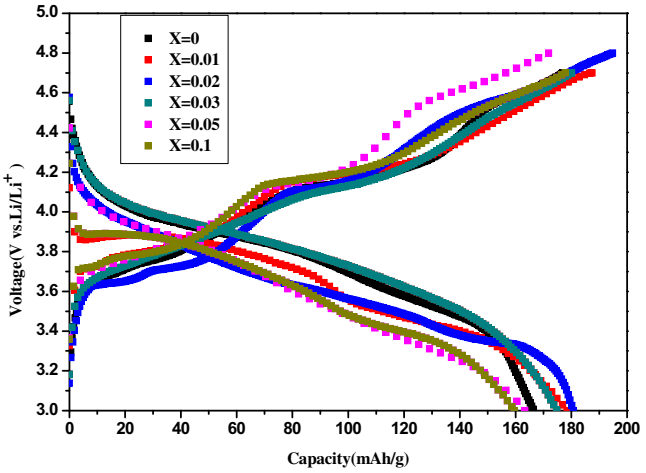

Fig. 5. Initial charge–discharge profiles of $Li_3V_{2-x}Ce_x(PO_4)_3/C$ (x = 0, 0.01, 0.02, 0.03, 0.05, 0.10) at the 0.2C rate in the voltage of 3.0–4.8 V.

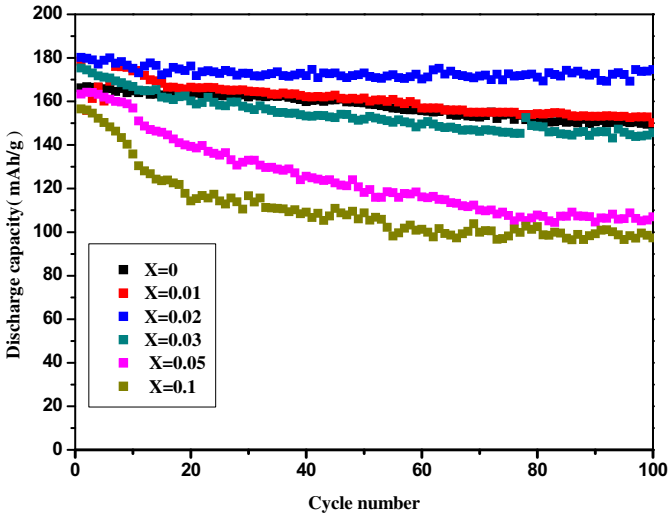

Fig. 6. Cycling performance of $Li_3V_{2-x}Ce_x(PO_4)_3/C$ (x = 0, 0.01, 0.02, 0.03, 0.05, 0.10) at 0.2C discharge rate between 3.0 V and 4.8 V.

significantly improve the cycling stability of the cathode [27]. However, as the doping content of Ce exceeded 0.03 (e.g., $x = 0.05$ and $x = 0.1$), impurity phases such as $Ce(NO_3)_3$, CeO_2 and Li_3PO_4 appeared. Furthermore, the entire diffraction spectrum was right-shifted with increase in the doping concentration (x value).

Additionally, from elemental analysis (not shown here), we determined the carbon content of $Li_3V_{2-x}Ce_x(PO_4)_3/C$ (x = 0, 0.01, 0.02, 0.03, 0.05, 0.10) samples to be ~11.37%, ~10.68%, ~10.02%, ~11.07% and ~9.99%, respectively. Such high concentration of carbon is essential in maintaining an effective inter-particle electrical contact [28]. However the XRD study (Fig. 2) did not reveal any peaks that could be associated with carbon in the $Li_3V_{2-x}Ce_x(PO_4)_3/C$ (x = 0, 0.01, 0.02, 0.03, 0.05, 0.10) composites, which indicates that the residual carbon is amorphous [29]. As a result, the presence of the amorphous residual carbon does not affect the crystalline structure of $Li_3V_{2-x}Ce_x(PO_4)_3$ and will serve to improve the electronic conductivity and the mechanical stability of $Li_3V_2(PO_4)_3$ composites.

3.3. Morphology of the $Li_3V_{2-x}Ce_x(PO_4)_3/C$ composites

The SEM images of the Ce doped and undoped samples are shown in Fig. 3(a)–(f). From SEM observations, all the samples show a flake-like morphology. The $Li_3V_2(PO_4)_3/C$ particles are about 1 μm in diameter and slightly agglomerated with each other as shown in Fig. 3(a) while the size of $Li_3V_{2-x}Ce_x(PO_4)_3/C$ (x = 0.01, 0.02, 0.03, 0.05, 0.10) particles is smaller and more uniform compared to the baseline with diameters of ~500 nm as indicated in Fig. 3(b)–(f). Interestingly, there are some nanorods in the undoped samples (inset of Fig. 3(a)). However, these nanorods cannot be detected in the doped samples which indicates that the addition of Ce influences the geometry and shape of the particles. This result is similar to what has been previously observed in Nb-doped $Li_3V_2(PO_4)_3/C$ [30]. Among the doped samples, the $Li_3V_{1.98}Ce_{0.02}(PO_4)_3/C$ composite has the smallest particle size (i.e. highest specific surface area) and a uniform morphology; we expect that such a microstructure will facilitate the penetration of the electrolyte ensuring better wettability and thereby shortening the diffusion distance of lithium ions from the cathode bulk phase to the electrolyte.

The image of TEM and HRTEM of the sample is shown in Fig. 4(a)–(h). From the TEM observation, the morphology and particle size of all the samples were found to be consistent with the SEM imaging shown in the previous figure. As compared to the smooth surface of pure $Li_3V_2(PO_4)_3$, it can be seen that the thickness of the amorphous carbon layer is ~5–10 nm on the surface of the $Li_3V_2(PO_4)_3$ and $Li_3V_{1.98}Ce_{0.02}(PO_4)_3$ grains. Such a conductive carbon network could provide good grain-to-grain electronic contact, thereby reducing the grain-to-grain electrical contact resistance leading to an improvement in electrochemical properties.

3.4. Electrochemical properties of $Li_3V_{2-x}Ce_x(PO_4)_3/C$ composites

The initial charge–discharge curves of $Li_3V_{2-x}Ce_x(PO_4)_3/C$ (x = 0, 0.01, 0.02, 0.03, 0.05, 0.10) samples at a charge/discharge rate (C-rate) of ~0.2C in the voltage range of 3.0–4.8 V are presented in Fig. 5. As can be seen in Fig. 5, almost all the samples obtained exhibit four voltage plateaus at around ~3.60, ~3.70, ~4.10 and ~4.60 V in the charge process, and three voltage plateaus around ~3.57, ~3.65, and ~4.1 V in the discharge process, which correspond to a sequence of phase transition processes in $Li_xV_2(PO_4)_3$ (x = 3.0, 2.5, 2.0, 1.0) [31]. It 2can also be seen that the initial discharge capacities of

Table 1
Electrochemical properties of $Li_3V_{2-x}Ce_x(PO_4)_3/C$ samples at 0.2C rate between 3.0 V and 4.8 V.

Samples	Initial charge capacity (mAh g^{-1})	Initial discharge capacity (mAh g^{-1})	Coulombic efficiency (%)	Discharge capacity after 100 cycles (mAh g^{-1})	Discharge capacity retention 100 cycles (%)
$Li_3V_2(PO_4)_3/C$	~176.9	~166.4	~94	~150.6	~90.4
$Li_3V_{1.99}Ce_{0.01}(PO_4)_3/C$	~187.4	~176.5	~95	~154.2	~87.3
$Li_3V_{1.98}Ce_{0.02}(PO_4)_3/C$	~191.8	~180.7	~94	~171.6	~94.0
$Li_3V_{1.97}Ce_{0.03}(PO_4)_3/C$	~179.4	~173.6	~96	~151.9	~87.5
$Li_3V_{1.95}Ce_{0.05}(PO_4)_3/C$	~171.9	~163.4	~94	~126.0	~77.2
$Li_3V_{1.9}Ce_{0.1}(PO_4)_3/C$	~177.9	~159.6	~90	~107.3	~67.2

$Li_3V_{2-x}Ce_x(PO_4)_3$/C composites depend significantly on the Ce-doping amounts. As shown in Table 1, the charge specific capacities of $Li_3V_{2-x}Ce_x(PO_4)_3$/C (x = 0, 0.01, 0.02, 0.03, 0.05, 0.10) are about ~176.9 mAh g^{-1}, ~187.4 mAh g^{-1}, ~191.8 mAh g^{-1}, ~179.4 mAh g^{-1}, ~171.9 mAh g^{-1}, and ~177.9 mAh g^{-1}, respectively, and the discharge capacities are about ~166.4 mAh g^{-1}, ~176.5 mAh g^{-1}, ~180.7 mAh g^{-1}, ~173.6 mAh g^{-1}, ~163.4 mAh g^{-1}, and ~159.6 mAh g^{-1} respectively. The corresponding coulombic efficiencies are ~94%, ~95%, ~94%, ~96%, ~94%, and ~90%, respectively. The high coulombic efficiencies are indicative of reversible phase transformations in $Li_3V_{2-x}Ce_x(PO_4)_3$/C associated with lithiation and delithiation steps, thereby ensuring repeatability and reversibility upon successive cycling [32]. However, it is clearly observed that the discharge specific capacity is enhanced considerably when the Ce-doping amount is x = 0.02. The high discharge capacity of $Li_3V_{1.98}Ce_{0.02}(PO_4)_3$/C can be attributed to the decrease of grain size and improved homogeneity as shown in Figs. 3 and 4. The electrochemical cycling performance of pristine and Ce-doped $Li_3V_{2-x}Ce_x(PO_4)_3$/C (x = 0, 0.01, 0.02, 0.03, 0.05, 0.10) samples at room temperature and at 0.2C rate in the voltage range of 3.0–4.8 V is shown in Fig. 6. As observed from Fig. 6, the specific capacities of $Li_3V_{2-x}Ce_x(PO_4)_3$/C (x = 0.01, 0.02, 0.03) composites display much better retention while $Li_3V_{1.95}Ce_{0.05}(PO_4)_3$/C ($x$ = 0.05) and $Li_3V_{1.9}Ce_{0.1}(PO_4)_3$/C ($x$ = 0.10) show significant capacity fade with cycle index. The discharge specific capacity of $Li_3V_{1.98}Ce_{0.02}(PO_4)_3$/C shows the best capacity retention among all the samples that were tested. After 100 cycles, the discharge specific capacities of $Li_3V_{2-x}Ce_x(PO_4)_3$/C (x = 0, 0.01, 0.02, 0.03, 0.05, 0.10) are ~150.6 mAh g^{-1}, ~154.2 mAh g^{-1}, ~171.6 mAh g^{-1}, ~151.9 mAh g^{-1}, ~126.0 mAh g^{-1}, and ~107.3 mAh g^{-1}, and the discharge capacity retention of the various samples after 100 cycles is ~90.4%, ~87.3%, ~94.9%, ~87.5%, ~77.2%, and ~67.2% respectively. These results indicate that the cycling stability of lithium vanadium phosphate can be significantly enhanced by doping with Ce, especially, by doping the optimal amount of Ce (x = 0.02). This improved cycling stability can be attributed to the monoclinic structure of $Li_3V_2(PO_4)_3$/C stabilized by Ce^{3+} doping. On the other hand, higher Ce contents such as x = 0.05 and x = 0.1 lead to reduced stability of the $Li_3V_2(PO_4)_3$/C cathode material presumably due to impurity phases that are nucleated in the material. To sum up, when both high initial capacity and capacity retention rate are considered, $Li_3V_{1.98}Ce_{0.02}(PO_4)_3$/C shows significantly better electrochemical behavior among all the samples that were tested including the baseline (un-doped) $Li_3V_2(PO_4)_3$.

The rate performance of the $Li_3V_2(PO_4)_3$/C and Ce doped $Li_3V_{1.98}Ce_{0.02}(PO_4)_3$/C is compared in Fig. 7. For the $Li_3V_2(PO_4)_3$/C sample, a specific capacity of ~158.4 mAh g^{-1} is obtained at ~1C rate. The specific capacity drops to ~96% of this value when the operating C-rate is increased to ~2C. The Ce doped $Li_3V_{1.98}Ce_{0.02}(PO_4)_3$/C delivers ~171.3 mAh g^{-1} at ~1C rate and retains a capacity of ~165.1 mAh g^{-1}(~97%) when the C-rate is increased from ~1C to ~2C. However when the rate is increased from ~5C to ~10C, there is a significant difference in the specific capacity between the $Li_3V_2(PO_4)_3$/C and Ce doped $Li_3V_{1.98}Ce_{0.02}(PO_4)_3$/C samples. The specific discharge capacity is ~120.4 mAh g^{-1} (~70%) for the Ce doped $Li_3V_{1.98}Ce_{0.02}(PO_4)_3$/C, while the pristine $Li_3V_2(PO_4)_3$/C only shows a specific capacity of ~83.0 mAh g^{-1} (~52%) when the C-rate is 10C. It was also found that the Ce doped $Li_3V_{1.98}Ce_{0.02}(PO_4)_3$/C can still deliver ~160.7 mAh g^{-1} (~94% retention) when the C-rate is brought back to 1C after 10C, while the $Li_3V_2(PO_4)_3$/C sample shows a significantly lower capacity of ~141.3 mAh g^{-1} (~88%). Faster lithium ion migration and more uniform particle distribution via the microwave assisted sol–gel method are responsible for the obtained high-rate performance after the Ce doping. The above results suggest that at the higher rates (5C/10C), the electrochemical dynamics are influenced by the

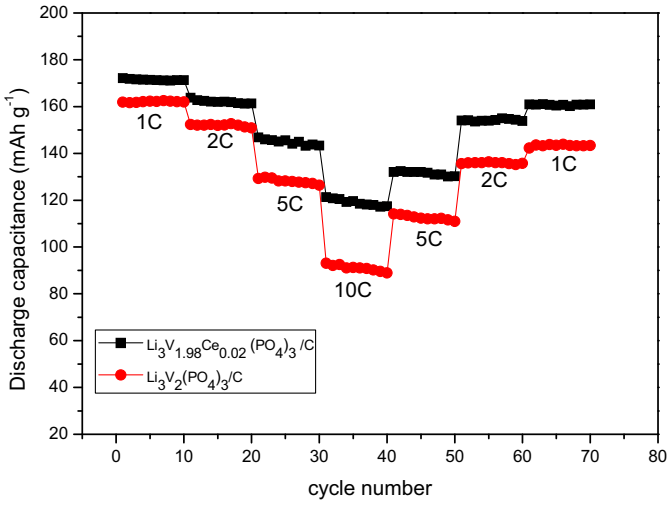

Fig. 7. Cycling performance of $Li_3V_2(PO_4)_3$/C and $Li_3V_{1.98}Ce_{0.02}(PO_4)_3$/C at different discharge rates of 1C, 2C, 5C, 10C, respectively, between 3.0 V and 4.8 V.

Li^+ diffusion in the bulk material rather than only by the electrochemical reaction rate.

Electrochemical impedance spectra measurements were also performed in order to better understand the kinetics of the $Li_3V_2(PO_4)_3$/C and the Ce-doped $Li_3V_{1.98}Ce_{0.02}(PO_4)_3$/C electrodes (Fig. 8). The inset equivalent circuit is used to simulate the impedance spectra. The high frequency region corresponds to the interfacial resistance at the surface of the cathode and its intercept is associated with the electrolyte resistance (R_e). The middle frequency semicircle is attributed to the charge–discharge process, which includes the particle-to-particle resistance (R1), capacitance at the electrode–electrolyte interface (CPE1), charge transfer resistance (R2) and the double-layer capacitance (CPE2). The low frequency semicircle represents the diffusion of lithium ion in the bulk of the electrode and this process is associated with the Warburg impedance (W1). As shown in Fig. 8, the charge-transfer resistance of the $Li_3V_{1.98}Ce_{0.02}(PO_4)_3$/C composite (~138.2 Ω) is significantly lower than that of the $Li_3V_2(PO_4)_3$/C (~267.9 Ω), which we expect is associated with the increase in electron conductivity associated with the Ce doping. Another interesting observation

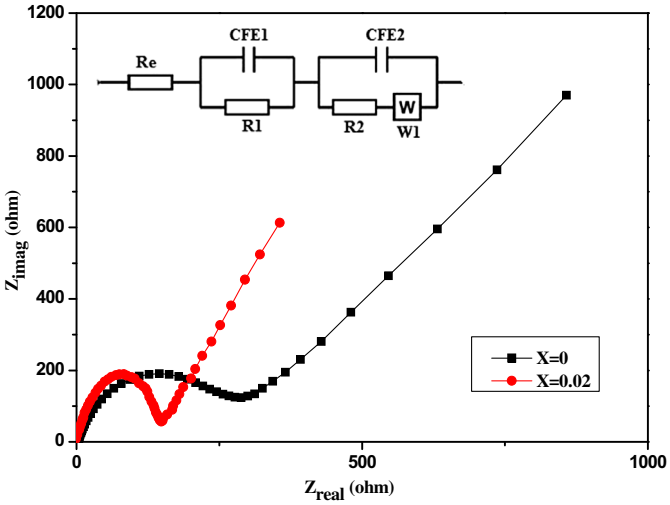

Fig. 8. Impedance spectra of the $Li_3V_2(PO_4)_3$/C and $Li_3V_{1.98}Ce_{0.02}(PO_4)_3$/C composites. Inset: Equivalent circuit corresponding to the impedance diagrams.

made from the impedance spectra is the low impedance associated with diffusion of lithium ions (low frequency spike) in Ce-doped $Li_3V_{1.98}Ce_{0.02}(PO_4)_3$/C. The low impedance can be attributed to higher surface area, uniform particle size distribution and better electrolyte wettability associated with microwave irradiation of the composite material. The aforementioned factors translate to greater accessibility to active sites for the lithium ions, shorter diffusion distances and quicker lithium ion diffusion, thereby explaining the significantly better rate capability of the Ce-doped $Li_3V_{1.98}Ce_{0.02}(PO_4)_3$/C composite electrode.

4. Conclusions

In this study, $Li_3V_2(PO_4)_3$/C and Ce-doped $Li_3V_2(PO_4)_3$/C composites are synthesized by a facile microwave assisted sol–gel method. The influence of Ce doping on the structural and electrochemical characteristics of $Li_3V_2(PO_4)_3$/C is analyzed. We show that small amounts of Ce ions can be incorporated into the crystal structure of $Li_3V_2(PO_4)_3$/C and the resulting composite exhibits smaller particle size, lower electron-transfer resistance, and faster lithium ion migration kinetics, which are attributed to Ce doping. At low rates, the Ce-doped $Li_3V_{1.98}Ce_{0.02}(PO_4)_3$/C composite delivers a stable specific capacity of ~170 mAh g^{-1} for over 100 cycles. At high rates (e.g. 10C), the Ce-doped composite is still able to deliver stable capacities of up to ~120 mAh g^{-1} which was found to be ~60% greater than its un-doped ($Li_3V_2(PO_4)_3$/C) counterpart.

Acknowledgments

Z.Y. acknowledges funding support by the National Natural Science Foundation of China (Grant Nos. 20963007, 21263016). N.K. acknowledges funding support from the USA National Science Foundation (Award 0969895) and the John A. Clark and Edward T. Crossan Chair Professorship from the Rensselaer Polytechnic Institute. N.K. and I.O. also acknowledge funding support by the International Cooperation of the Korea Institute of Energy Technology Evaluation and Planning (KETEP) grant funded by the Korea Government Ministry of Knowledge Economy (No. 20128510010050).

References

[1] L. Shen, H. Li, E. Uchaker, Nano Lett. 12 (2012) 5673.
[2] M. Armand, J.M. Tarascon, Nature 451 (2008) 652.
[3] J. Yan, W. Yuan, Z.Y. Tang, J. Power Sources 209 (2012) 251.
[4] Y.N. Ko, H.Y. Koo, J.H. Kim, J.H. Yi, J.H. Lee, J. Power Sources 196 (2011) 6682.
[5] K. Nagamine, T. Honma, T. Komatsu, J. Power Sources 196 (2011) 9618.
[6] A. Pan, D. Choi, J.G. Zhang, S.B.W. Arey, J. Power Sources 196 (2011) 3646.
[7] Y.Q. Qiao, X.L. Wang, Y.J. Mai, J.Y. Xiang, J. Power Sources 196 (2011) 8706.
[8] N.A. Koratkar, I. Chopra, AIAA J. 38 (2000) 1113.
[9] C. Dai, Z. Chen, H. Jin, X. Hu, J. Power Sources 195 (2010) 5775.
[10] A.K. Padhi, K.S. Nanjundaswamy, J.B. Goodenough, J. Electrochem. Soc. 144 (1997) 1188.
[11] M.Y. Saidi, J. Barker, H. Huang, J.L. Swoyer, G. Adamson, Electrochem. Solid-State Lett. 5 (2002) A149.
[12] Y.Q. Qiao, J.P. Tu, Y.J. Mai, L.J. Cheng, X.L. Wang, J. Alloys Compd. 509 (2011) 7181.
[13] H. Liu, P. Gao, J. Fang, G. Yang, Chem. Commun. 47 (2011) 9110.
[14] T. Jiang, Y.J. Wei, W.C. Pan, Z. Li, X. Ming, G. Chen, J. Alloys Compd. 488 (2009) L26.
[15] Q.Q. Chen, T.T. Zhang, X.C. Qiao, D.Q. Li, J.W. Yang, J. Power Sources 234 (2013) 197.
[16] S. Zhang, Q. Wu, C. Deng, F.L. Liu, M. Zhang, F.L. Meng, H. Gao, J. Power Sources 218 (2012) 56.
[17] Y.Q. Qiao, J.P. Tu, X.L. Wang, C.D. Gu, J. Power Sources 199 (2012) 287.
[18] Y.Q. Qiao, J.P. Tu, X.L. Wang, D. Zhang, J.Y. Xiang, Y.J. Mai, C.D. Gu, J. Power Sources 196 (2011) 7715.
[19] Y.H. Chen, Y.M. Zhao, X.N. An, J.M. Liu, Electrochim. Acta 54 (2009) 5844.
[20] Q. Kuang, Y.M. Zhao, X.N. An, J.M. Liu, Electrochim. Acta 55 (2010) 1575.
[21] J.S. Huang, L. Yang, K.Y. Liu, Y.F. Tang, J. Power Sources 195 (2010) 5013.
[22] J. Barker, R.K. Gover, P. Burns, A. Bryan, J. Electrochem. Soc. 154 (2007) A307.
[23] L.L. Zhang, X. Zhang, Y.M. Sun, W. Luo, X.L. Hu, J. Electrochem. Soc. 158 (2011) A924.
[24] Q. Kuang, Y.M. Zhao, Z.Y. Liang, J. Power Sources 196 (2011) 0169.
[25] G. Yang, H.D. Liu, H.M. Ji, J. Power Sources 195 (2012) 5374.
[26] G. Liu, Y. Liu, L.Q. Liu, J. Inorg. Mater. 27 (2012) 1017.
[27] H.C. Shin, W.I. Cho, H. Jang, J. Power Sources 159 (2006) 1383.
[28] X. Yang, W.K. Zhang, H. Huang, Y.P. Gan, Mater. Sci. Eng. B. 176 (2011) 633.
[29] M.Y. Saidi, J. Barker, H. Huang, J.L. Swoyer, G. Adamson, J. Power Sources 119 (2003) 266.
[30] M. Koltypin, V. Pol, A. Gedanken, D. Aurbach, J. Electrochem. Soc. 154 (2007) A605.
[31] L. Mai, L. Xu, C. Han, X. Xu, Y. Luo, S. Zhao, Y. Zhao, Nano Lett. 10 (2010) 4750.
[32] W. Wang, H. Wang, S. Liu, J. Huang, J. Solid State Electrochem. 16 (2012) 2555.